FINAL REPORT

OTKA K 125409

Investigation of the effect of galvanic current generated by different metal implants for the ossification

Period: 01.09.2017 - 31.03.2023

Principal investigator: Prof. Zoltán Csernátony

Institute: Department of Orthopaedic Surgery, University of Debrecen

Address: 4032 Debrecen, Nagyerdei krt. 98.

E-mail: csz@med.unideb.hu

Phone: +36 52 255 815

INTRODUCTION

In trauma and orthopaedic practice, bone defects and fractures tend to heal according to plan, but when delayed fracture healing, or pseudarthrosis, occurs for any reason, it often presents a challenge to the clinician. The industry that manufactures implants for musculoskeletal surgery has also seen developments in implant design, surface treatment and metallurgical innovations. The surgeon performs a wide variety of metal-on-metal debonding, sometimes by choice and sometimes due to the necessity of the surgical situation or the lack of implants. During the healing process, bone resorption and bone formation have been observed in these situations. Our hypothesis is that one of the possible causes is the galvanic current that occurs between the different metal materials. The stimulation of fracture healing is a recurring area of research. Today, therapeutic practice consists of transcutaneous induction or, rarely, implantable electrical devices for bone-stimulating treatments; the inefficiency of these treatments does not cause complications, but rather they are considered ineffective. In this study, we want to verify, through animal experiments, whether the galvanic-electrical phenomenon that occurs between implants of different material quality affects bone healing, and if so, whether it stimulates or inhibits it, and what can be observed in different pairings. Our aim was to find an ideal metal-metal pairing that is beneficial to bone healing and can be used in the development of future implants.

We planned to carry out the research using animal experiments. We chose New Zealand Giant domestic rabbits as our experimental subjects because the size of these animals were suitable for our investigations. We wanted to perform the planned studies on both femurs of the experimental subjects.

In the first year of the project, according to our work plan, we had several meetings and multidisciplinary consultations with those involved in our research. We reviewed the relevant literature, planned the experimental set-up, scheduled the operations, examinations, methods, etc.

We developed the experimental design and insertion technique:

- We determined the type and size of screws to be used in the studies.
- We planned to place two cortical screws in the diaphysis of the femur, using conventional KFI cortical screws (diameter 2.7 mm). This type and size of screw could be safely inserted without risk of fracture.
- We have designed some special custom-made devices to aid insertion.

We carried out preliminary measurements of static current in vitro on fresh frozen rabbit bones.

- We measured the conductivity of the bone and the impedance of the screw alloys.
- We measured the static current between the screws.
- We made electron microscopic scans of the screws to study their structures.

We carried out preliminary radiological studies.

- We scanned fresh bone using CT and MRI.
- We determined the appropriate parameters for the studies.
- We made 3D CT reconstructions of the model to visualise the defect.
- We developed an evaluation method to follow the bone healing and to estimate the volume change of the bone in the area of the bone defect during healing.

In the second year of the project, it took a long time for our ethical application for animal experiments to be approved; the application had to be amended several times. We had the final decision in August 2019, which allowed the surgeries to go ahead. We got permission to operate on 55 rabbits, so the experimental methods had to be modified. We had to change the number of animals in the experimental groups.

Unfortunately, the site of the animal experiments, the Department of Operative Techniques and Surgical Research of our university, was under reconstruction, so the experiments with live animals could not start until autumn 2019.

We have improved the experimental setup and insertion technique. Previously, we'd planned to place two cortical screws in the diaphysis of the femur. During the further operations, based on some relevant publications, we've tried a different region for the operation, the distal metaphysis of the femur. After the surgeries we decided that this was the preferred site because it was easier to perform a minimally invasive

approach, the bone healing was better in this site, the animals tolerated it better and the results were more comparable. We hadn't changed the type of implants used, which were conventional KFI cortical screws (diameter 2.7mm). We've found that this type and size of screw can be safely inserted in this region without risk of fracture.

After the COVID pandemic, we could start the surgeries in the early summer of 2021 with surviving animals.

In the experiment, two bicortical screws of 2.7 mm diameter were implanted in the femurs of the subjects at the same distance (16 mm) in each animal, and a monocortical defect of 2 mm diameter was created between the two screws at the same distance from the two screws. The animals were divided into 5 groups. In all five groups, the right femur of the animals served as a control compared to the left femur of the tested animals. In the first group, the control was the bone defect created on the right side without implantation. In the other groups, the control for the side tested was the stainless steel implants(SS) on the right side with a defect created between them. In the study, implants made of titanium alloy(Ti), gold(Au) and platinum(Pt) were tested in combination with stainless steel screws. The experimental arrangement of each group is shown in Figure 1.

	Experimental side femur	**Control side femur**
1. group	stainless steel-stainless steel	bone defect only
2. group	stainless steel-stainless steel	stainless steel-stainless steel
3. group	stainless steel-titanium	stainless steel-stainless steel
4. group	stainless steel-gold	stainless steel-stainless steel
5. group	stainless steel-platinum	stainless steel-stainless steel

Figure 1. Experimental groups

The operations were performed at the Department of Surgical Technique and Research of the Medical Faculty of the University of Debrecen. The operations were carried out in accordance with current legislation and ethical guidelines.

Steps of the surgeries is shown below.

1. Surgical approach

2. Aiming and drilling



3. Implantation of screws and electric device

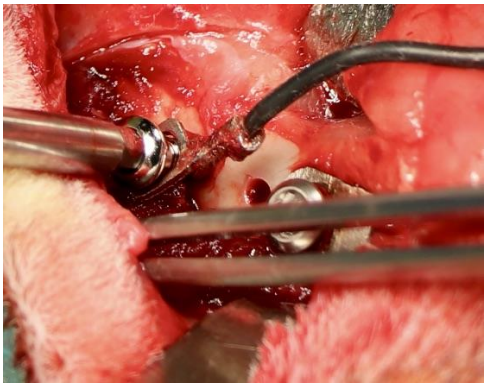


4. Skin closure

In all cases, the polarity of the electrical measurement device was chosen so that the cathode was positioned proximal to the defect and the anode distal to the defect. In parallel with the animal studies, data collection and processing has begun. During the project we developed a device that could be implanted under the skin of the rabbits to continuously clot the voltage in the bone. We also recorded the animals' temperature, acceleration during movement and the charge level of the battery that powered the multifunctional device.

MEASUREMENTS AND RESULTS

1. Galvanic voltage measurements

Materials and methods

During our examination, we performed animal experiments on rabbits to investigate the healing process of artificially created bone defects, by measuring, recording, and evaluating the galvanic voltage between metal components. The electrolyte of the galvanic cell was the extracellular fluid of the tissues of the test animal. Figure 2. shows the arrangement for measuring the galvanic voltage on the femur bone.

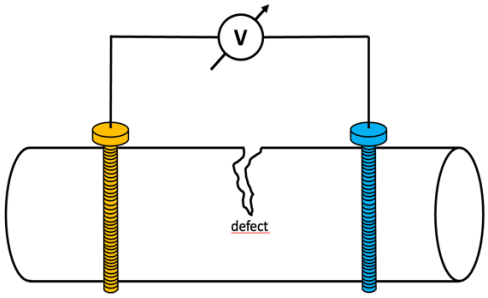

Figure 2. Electrode arrangement for measuring galvanic voltage

A special, implantable elctronical measurement unit had to been developed to perform the electronic voltage measurements.

The electronic measuring device to be developed must therefore meet additional requirements

- The electronic measurement and data transmission device, which is placed under the skin of the living animal during the surgical procedure, must not adversely affect the animal's quality of life during the experiment.
- The built-in battery must provide sufficient power for the entire duration of the measurement.
- A special case had to be designed that was hermetically sealed, tissue friendly and small enough to be placed under the animal's skin.
- The radio communication had to be reliable to work through living skin tissue.

During the electronics design phase, preliminary experiments were carried out to select the type of radio communication, the best microcontroller and the optimal battery power supply.

Another very important choice is the type of radio communication between the sensor and the transmitter. In the end, we chose standard Bluetooth communication because there are many integrated radio solutions available, and our preliminary experiments proved that 1mW output power is sufficient for safe radio signal reception from under the animal's skin tissue.

It is also very important to know in advance what the power consumption of the system will be. During the four weeks of the experiment, it is not necessary to collect data more frequently than every 8 seconds. It is possible that 8 seconds is too dense, but even in the event of a single data loss for any reason, the backup is guaranteed.

The microcontroller has been programmed to operate in a periodic manner, which includes a normal data measurement and transmission phase and a sleep phase. During the sleep phase, not only does the microcontroller enter a low-power mode, but so do all the other components. The whole system consumes only a few microamps. The active time in the 8 seconds is only 25msec. Using this technology, we have

demonstrated that a single Li 3V CR2032 battery cell can power the entire system for approximately four months. All selected system components are capable of operating from 3.2V to 2.7V, eliminating the need for an additional voltage regulator in the power scheme.

The complete measurement system is shown in Figure 3.

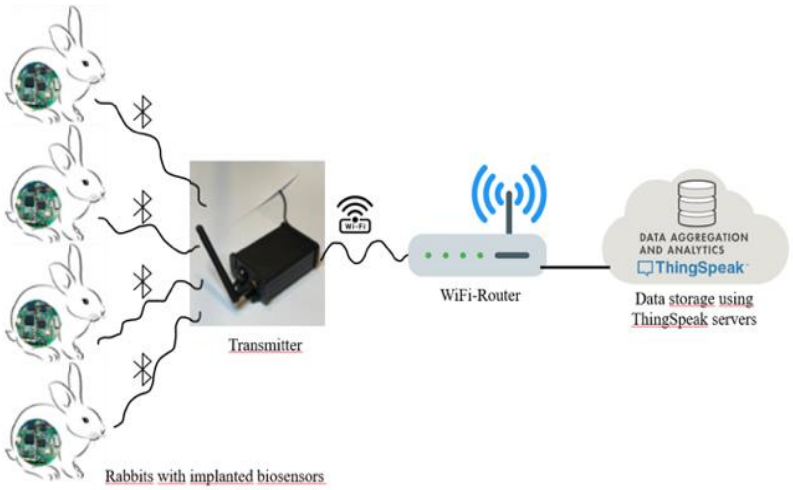

Figure 3. The measurement system

As well as measuring the galvanic voltage level, we also measured a number of other parameters, all of which were sent to the server. The following list contains all the components of the data packets:

- Identification number of the given sensor.
- Time stamp of the data.
- The galvanic voltage between the contacts.
- The actual temperature of the whole system, which was of course the temperature of the animal.
- The magnitude of the acceleration vector of the system, which contained information about the actual movement of the animal.
- The actual battery voltage, informing the user of the "health" of the battery.

All data packets are stored on a server.

The Electronics

The complete block diagram of the sensor electronics is shown in Figure 4.

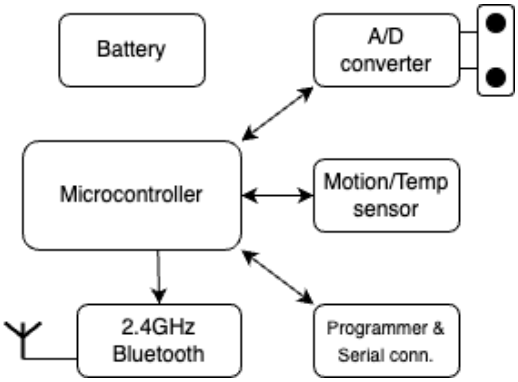

Figure 4. The complete measuring system

The microcontroller
The Microchip picoPower® 8-bit AVR® RISC-based microcontroller was chosen to control the entire data acquisition system [3]. The controller has six low power modes (1μA@3V) and low normal operating current (1.5mA@4MHz). The 8 second wake-up time can be easily programmed using the watchdog timer.

The Bluetooth interface
We chose the NORDIC nRF24L01 integrated circuit [4]. This is a low power version of the nRF24 family, which means that the maximum output power is 1mW. According to our preliminary measurements, this power is sufficient to transmit the data packet. This device has 128 individual RF channels, so we were able to assign an RF channel to each sensor. We placed the antenna and its matching network directly on the PCB to minimise the overall size of the electronics.

The AD converter
There are some specific requirements when selecting the AD converter IC. The resolution should be high, at least 14 bits, the input range should be bipolar, and the maximum input level should be below +/-500mV. There was no need for high measurement speed, but the power consumption had to be low. In the end, the ADS 1116 [5] was chosen. The most important parameters for our application are 16 bit resolution, bipolar +/-512mV input voltage range, two channel programmable differential input amplifier stage and internal reference. Its normal operating current is 150μA.

The motion/temperature sensor
There was no particular need to measure animal movement accurately. All we wanted to know was whether the animal was moving a lot or not at all. It is assumed that the value of the galvanic voltage can be affected by sudden movement, so this data should be filtered out. As the movement can be in any direction, we need to use a three-dimensional sensor and only the magnitude of the acceleration vector is calculated and transmitted.
The final choice was the MPU6050 motion sensor. We only used the acceleration and temperature sensors. The accuracy of the accelerometer is high, but the performance of the temperature sensor is not. Its resolution is high, but its linearity is low and it also has a relatively large offset error. In our animal temperature measurement application, the temperature changes were very small and after a single offset calibration, the absolute accuracy met the requirements.

The PCB design
The smallest possible overall size was a very important consideration in the design of the PCB. In the end, a 25mm diameter flat disc design was chosen (Figure 5.)

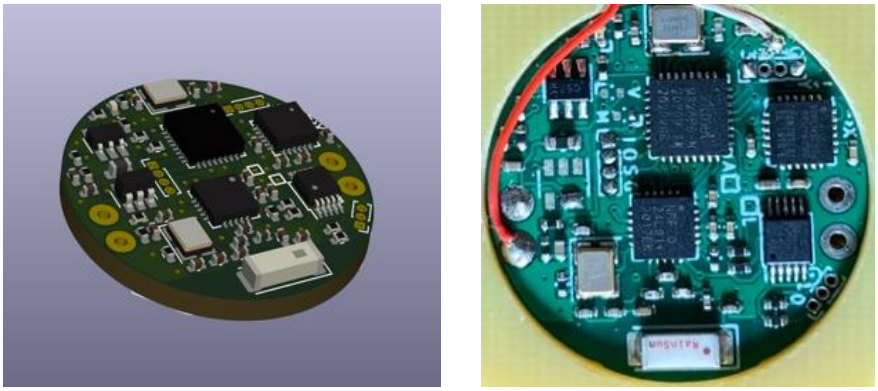

A B
Figure5. The PCB design(A) and the soldered real version(B)

To minimise the size of the PCB, the Bluetooth radio IC, chip antenna and antenna matching network were placed directly on the panel. It was certainly a challenge to maximise the radiated output power of the antenna and to minimise the detuning effect from the actual channel frequency.

The final verison can be seen in Figure 6.

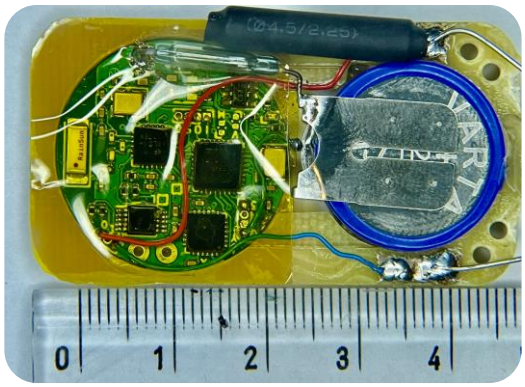

Figure 6. The Final version of microcontroller

In order to make all the electronics as thin as possible, we placed the batteries next to the electronics in a machined frame made of FR4 PCB material. The hermetic housing for the system is made of tissue-friendly plastic material and is produced using 3D printing technology The packaged electronics also needed to be sterilized before use. (Figure 7.)

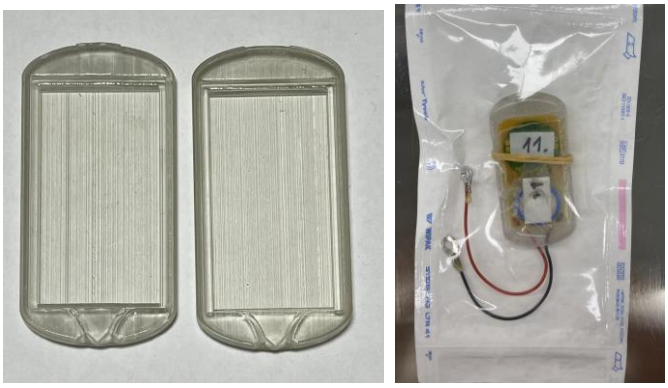

A B

Figure 7. Hermetic housing(A) and the sterilized, ready to implant device(B)

Following the surgical implantation of the electronic device, data began to be collected.

Typical measurement results can be seen in Figure 8.

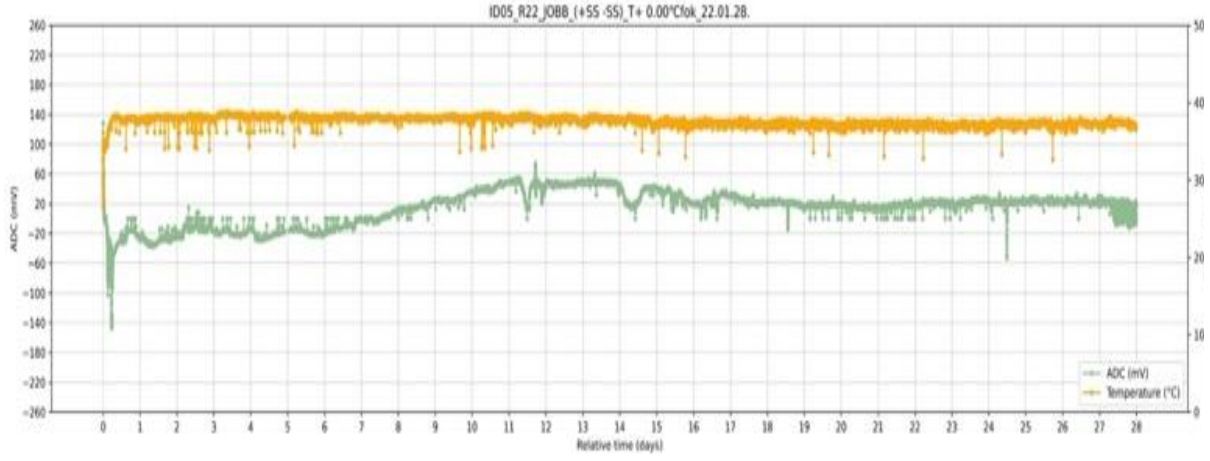

Figure 8. Measurement result sample

The measurement data shows some results of one month of continuous measurement. A systematic change in the measured galvanic voltage - after the initial transients - could be observed, while the temperature of the animal is quite constant.

Data processing

During the data filtering process, the following filtering operations are performed:

The ADC measurements gave a lot of false data, which were filtered out with the following solutions:

1. ADC values should be kept within the range +/- 260 mV. Thus the first filtering was applied to this.
2. additional spurious data were filtered by filtering out changes of more than -10 and 10 mV between two consecutive values in the data series.
3. The ADC values around zero also generated a lot of spurious data, these were filtered out by removing the +/- 0.5 mV range.

When generating the trendline, a polynomial line was fitted to the data. The degree of polynomial fit can be specified in the code. The Python 'polyfit' function determines the polynomial coefficients for both ADCs. The function 'np.linspace' calculates the x and y values representing the trendlines. The trend line functions have been plotted on the same graph and their corresponding spread values have been plotted.

Results

The measurement results show that a galvanic voltage is generated between the implants. The voltage values fluctuate strongly around the time of implantation, which may be due to mechanical effects during implantation. The voltage between implants was measured for both identical and different metal pairs, which is not surprising given the piezoelectric properties of bone tissue. After implantation, a negative voltage developed in the experimental setup, which changed to a positive voltage over time as bone healing progressed, and then stabilised at a relatively constant level. Stable voltage values were reached around day 14. The nature of the voltage curves was similar for both the same and different metal pairs.

2. Mechanical examinations

Our aim was to measure the flexural strength of a normal rabbit femur with and without two screws and a monocortical hole of 2 mm diameter between them, in the same arrangement as during the operations of the animal experiment.

Materials and Methods

Femurs taken from the same animal were placed on a flat surface and a load applied at the centre of the diaphysis at a constant speed of 5 mm/min using a rounded loading part in an Instron 8874 materials testing machine. Experimental setup can be seen in Figure 9.

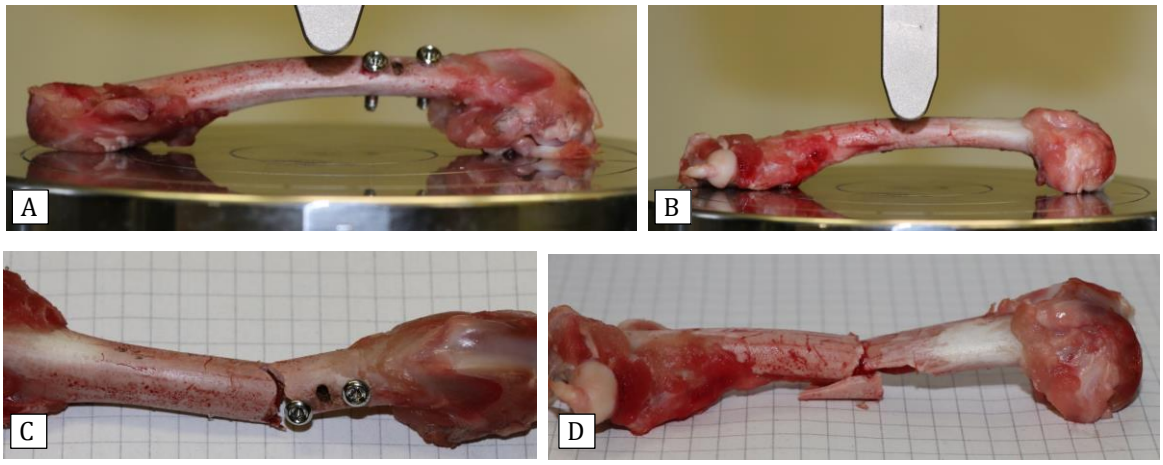

Figure 9. Loading of implanted rabbit femur (A) and intact rabbit femur (B) and fractures after loading to critical bending force in implanted rabbit femur (C) and intact rabbit femur (D)Results

The maximum average bending force was 310N for the healthy bone and 210N for the bone with the screws and the hole between them. The strength of the bone with the screws and the defect was therefore approximately 2/3 of that of the unaffected femur.

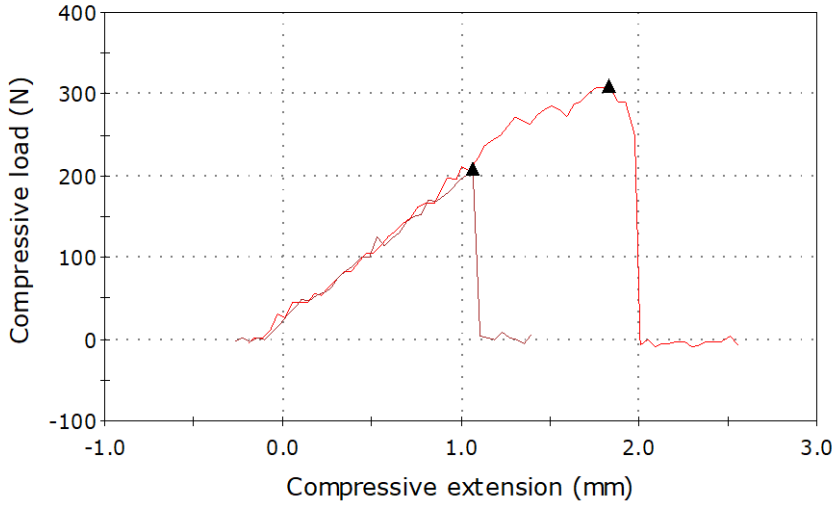

Figure 10. Deformation curve of implanted femur(black) and intact femur(red)

3. Radiological evaluation

Materials and methods

After the animals were sacrificed, the femurs were removed. The previously implanted screws were also removed and the bones were subjected to a CT scan.

Specifications of CT scans can be seen in Figure 11.

CT scan specifications	
Parameters	**Values**
Tube current	0,87 mA
Tube voltage	50kVp
Exposition time	300 ms
Pitch	1
Exposition[mAs]	0,261 mAs
Slice fitness	0,23 mm
Reconstruction	FBP
Reconstruction matrix/pixel size	438 × 438/250×250 µm

Figure 11. CT scan specifications

During the radial assessment, we measured the diameter of the residual defect created between the two previously inserted bones, the volume of callus formed, and the density of the bone tissue in the formed callus compared to the bone tissue in the same bone in the area not affected by the experiment.

3.1. Measuring the diameter of residual defect

The maximum diameter of the bone defect defined by the line Range of Interest (ROI) on the CT scans [mm] (Figure.12.).

Figure 12. Definig of the line Range of Interest (ROI)

3.2. Volume of the callus

The callus area (Ai) was delineated in each CT slice and multiplied by the CT slice thickness (0.23 mm). This gave a volume slice of the callus. These volume slices were summed to obtain the total callus volume (Figure 13.).

$$V_{callus} = \sum A_i \times 0{,}23mm$$

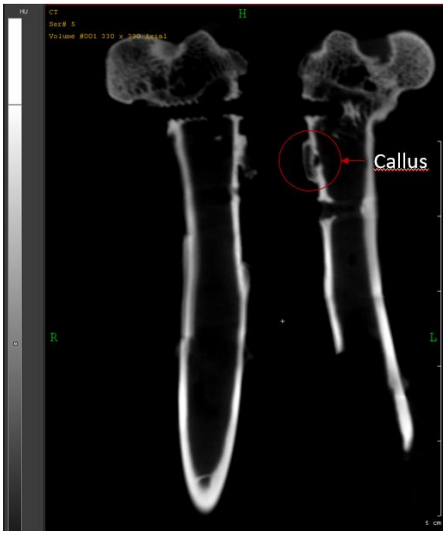

Figure 13. Callus formation on femur

3.3. Callus/bone density

In each CT scan, the reconstructed bone tissue is characterised by a number in HU (Hounsfield) units. This number is representative of the density of bone tissue, so we calculated the average HU values for callus and original bone. The ratio of the HU values for callus and bone gives an indication of how close the density of the bone tissue formed in the callus is to the density of healthy bone tissue. If this ratio is close to 1, it means that the bone density of the callus is close to that of healthy bone (Figure 14.).

$$C = \frac{\overline{HU}_{callus}}{\overline{HU}_{bone}};$$

The average callus and bone density are calculated using the following weighted average:

$$\overline{\boldsymbol{HU}_{\boldsymbol{callus}}} = \frac{\sum \boldsymbol{HU}(\boldsymbol{callus})_i \times \boldsymbol{A_i}}{\boldsymbol{A_{callus}}};$$

and

$$\overline{\boldsymbol{HU}}_{\boldsymbol{bone}} = \frac{\sum \boldsymbol{HU}(\boldsymbol{bone})_i \times \boldsymbol{A_i}}{\boldsymbol{A_{bone}}};$$

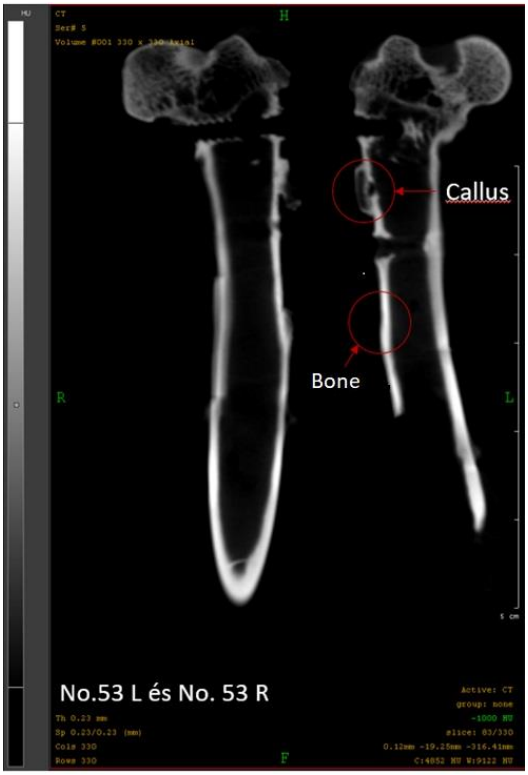

Figure 14. Bone and callus density ROI

Results

When looking at the residual bone defect diameter, the smallest average residual defect diameter was seen with the gold-steel and platinum-steel combinations, while the largest residual defect diameter was seen with the titanium-steel combination (Figure 15).

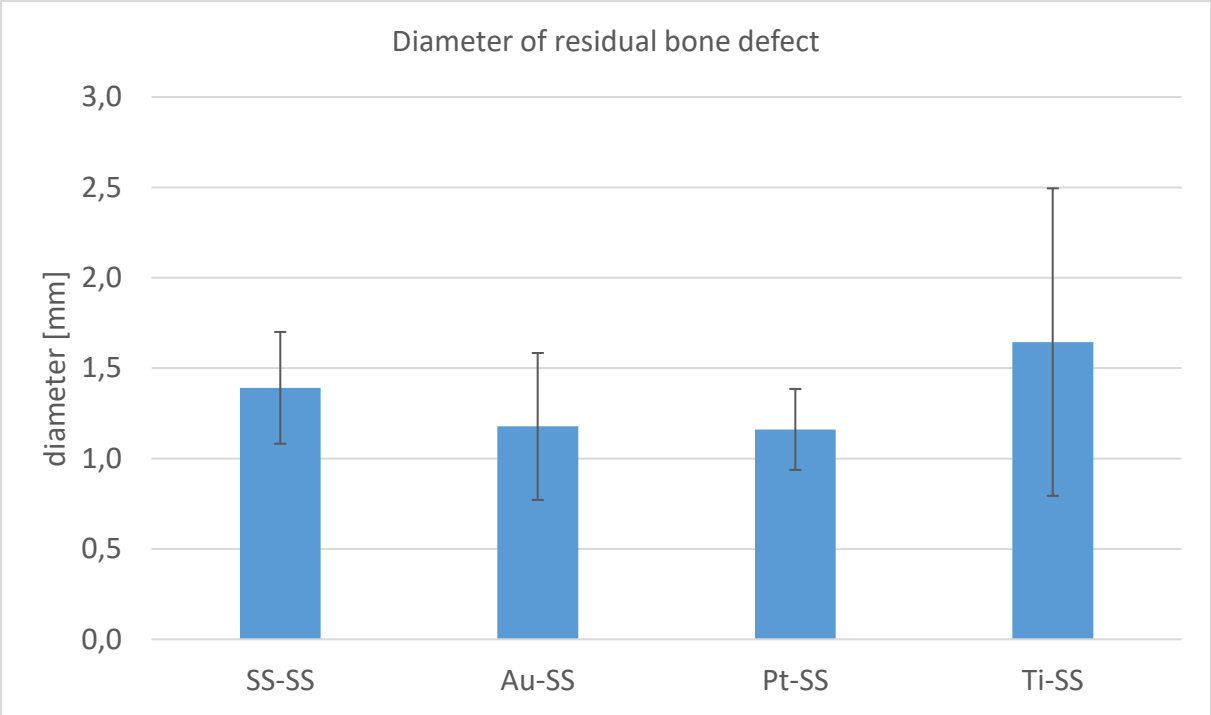

Figure 15. Average diameter of residual bone defect in case of different metal pairs(SS-stainless steel, Au- gold, Pt-platinum, Ti- titanium)

Examining the callus volumes, we found that the ss-ss and ti-ss metal pairs formed on average nearly equal amounts of callus, the AU-SS combinations formed about 20% less, while the PL-SS pairs formed about 50% less callus on average (Figure 16).

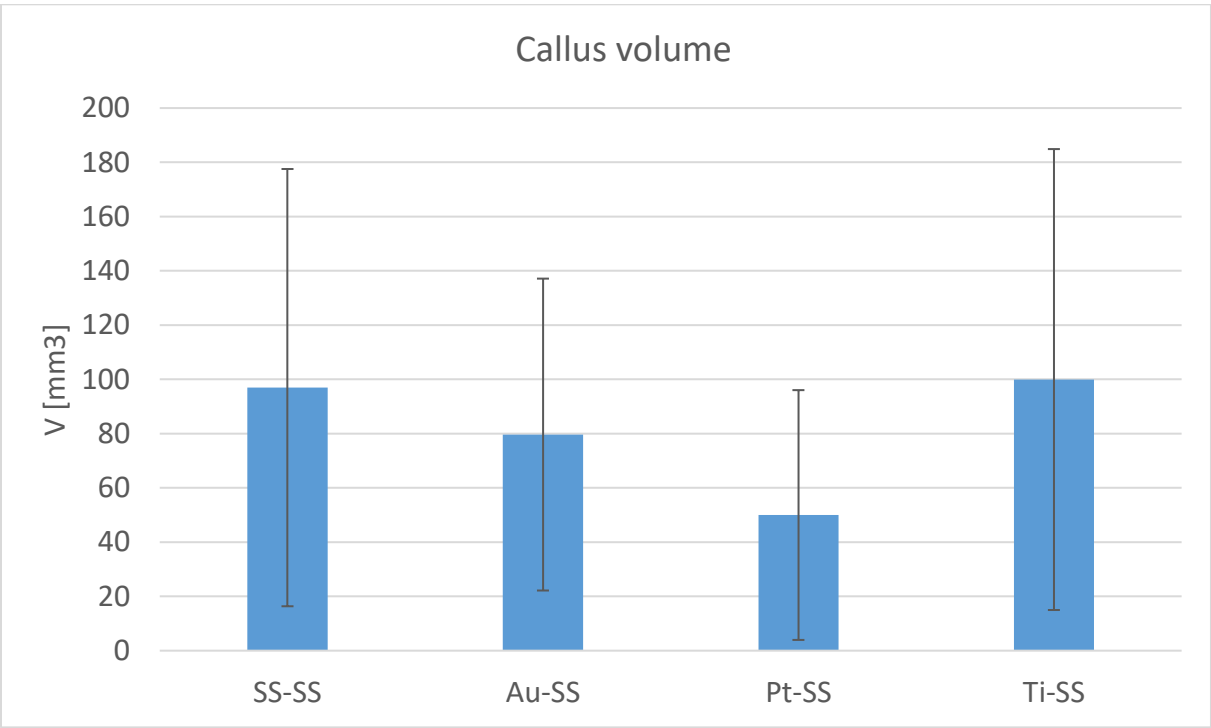

Figure 16. Average callus volume in case of different metal pairs(SS-stainless steel, Au- gold, Pt-platinum, Ti- titanium)

When comparing callus bone density, our experience has shown that the average density of the Pt-SS pairings is closest to that of intact bone tissue(0,55), with the other pairings having average densities about 10% lower (Figure 17.).

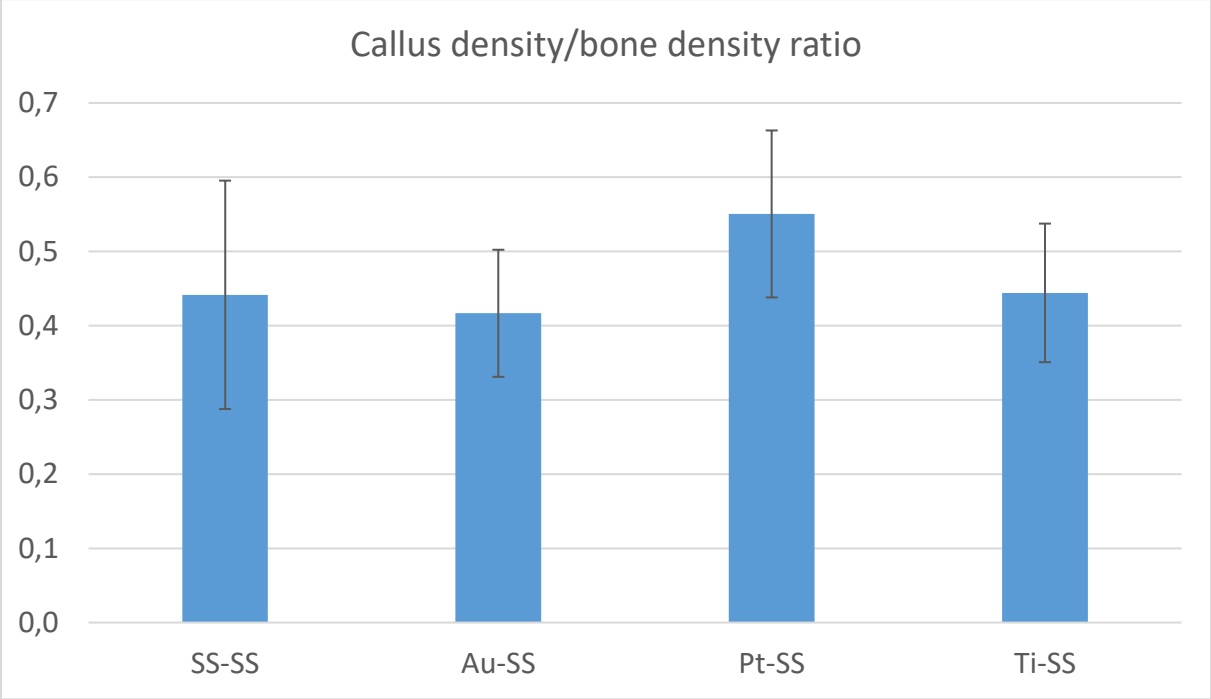

Figure 17. Average callus density/bone density ratio in case of different metal pairs(SS-stainless steel, Au-gold, Pt-platinum, Ti- titanium)

4. Histological examinations

Materials and methods

Light microscopic morphology

Bone samples from the same experimental groups were taken separately from the intact and examined (defect) areas. Samples were washed three times in PBS and fixed in a 4:1 mixture of absolute ethanol and 40% formaldehyde for 2 days, then kept in 4% EDTA decalcifying solution for 4 weeks. After decalcification, the samples were embedded in paraffin. Seven μm thick serial sections were prepared and hematoxylin-eosin staining (HE, Sigma-Aldrich, MO, USA) was performed for morphological analysis. The staining protocol was performed according to the manufacturer's instructions. Photomicrographs were taken using a DP74 camera (Olympus Corporation, Tokyo, Japan) on an Olympus Bx53 microscope (Olympus Corporation, Tokyo, Japan). Picrosirius red staining (Sigma-Aldrich, MO, USA) was used to examine collagen fibres in bones. In polarised light, samples were examined in an Olympus Bx53 polarisation microscope with constant exposure time and settings (Olympus Corporation, Tokyo, Japan) by rotating the light plane at λ/4. The integrated red and green pixel intensity was then determined using ImageJ 1.40g freeware.

Statistical analysis

Where appropriate, data are expressed as mean ± SEM. Statistical analysis was performed using Student's t-test, with the statistical method reporting significant differences between groups at $p<0.05$. * indicates significant difference between red and green fibres and # indicates significant difference between red/red or green/green experimental groups.

Collagen

In cortical bone, the expression and orientation of collagen type I also affects bone integrity and callus formation. Therefore, the presence of collagen was also detected by picrosirius staining. Under polarised light, collagen-positive fibres appear in two different colours, for example, thick collagen fibres appear red and thin collagen fibres appear green. The amount of red and green fibres is in proportion to callus formation.

Results

4.1. Bone defect only group

In the control cortical bone, normal histological architecture was detected, whereas on the side of the defects, Volkmann's canals and lamellar structure of collagens are not detectable (Figure 18.A). Picrosirius staining showed a stronger red colour in normal light (Figure 18.B) and in λ/4 rotated polarised light a stronger red and green colour in callus formation. In physiological cortical bone, red/thick collagen fibres were significantly more abundant than thin/green stained collagen fibres (Figure 18.C). In surgically induced defects, a significant increase in thick collagen fibres was detected, whereas a slight but not significant increase in thin collagen fibres was detected (Figure 18.C).

A. H&E staining

Control Investigated

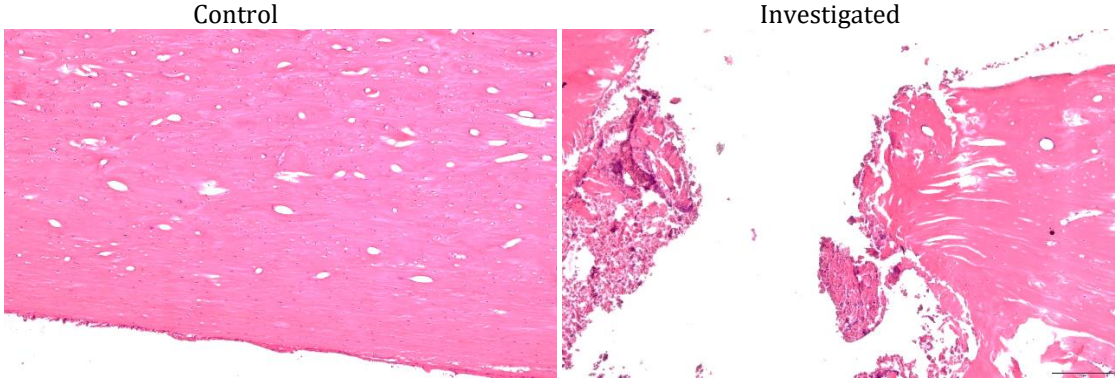

B. Picrosirius red staining

Control Investigated

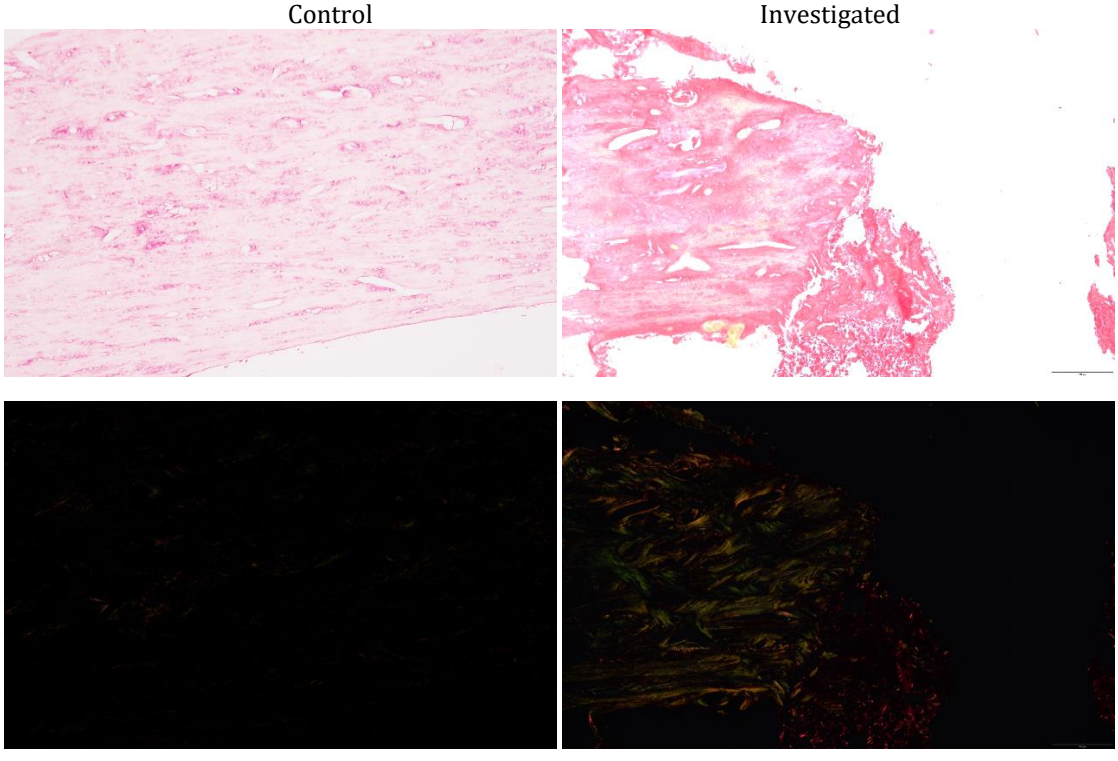

C. Red-green pixel ratio

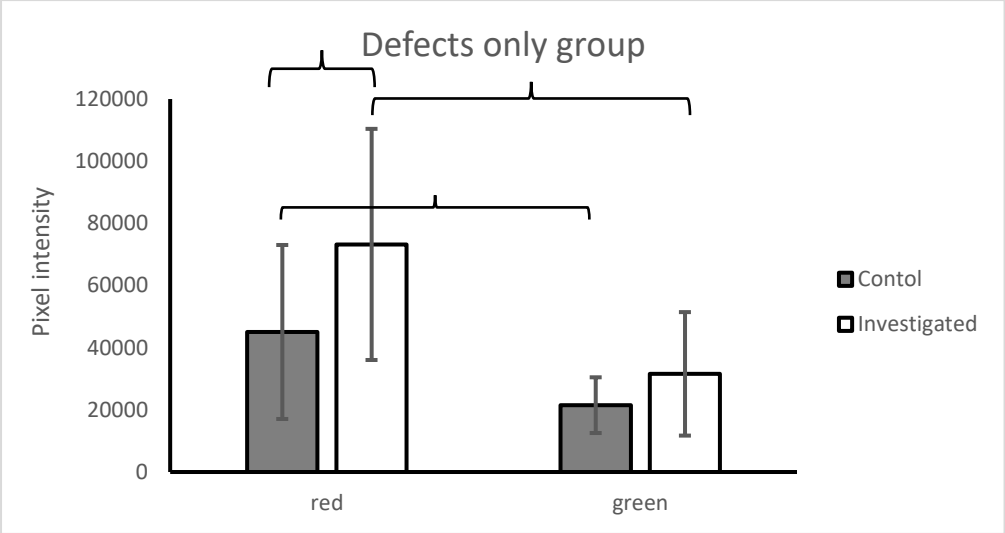

Figure 18. Examination of the organic matrix production of bone. Hematoxilin eosin (A) and picrosirius red (B) staining. Original magnification was 20×. Scale bar: 100 µm. Optical density (OD) of red and green pixels was determined in micrographs and normalised to control, unoperated bone samples (C). Asterisks indicate significant (*p<0.05) change in red or green pixel intensity compared to the corresponding control and (#p<0.05) change in red-red or green-green compared to the corresponding control in bone defect only group.

4.2. Stainless steel-stainless steel group

Similar to the previous experimental group, intact bone had normal histological characteristics (Figure 19.A) and callus formation was detected on the side of the stainless steel screws (Figure 19.A). Picrosirius staining showed similar results (Figure 19.B) with a strong red colour in polarised light on the side examined (Figure 19.B). After surgery between stainless steel (SS) screws, no significant change in the amount of thick collagen fibres was detected, but a significant reduction in the amount of thin collagen fibres was shown in the studied side (Figure 19.C).

A. H&E staining

Control Investigated

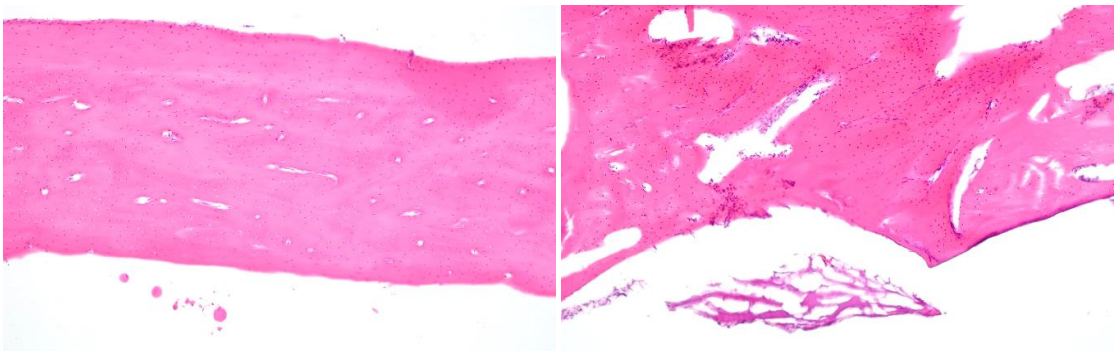

B. Picrosirius red staining

Control Investigated

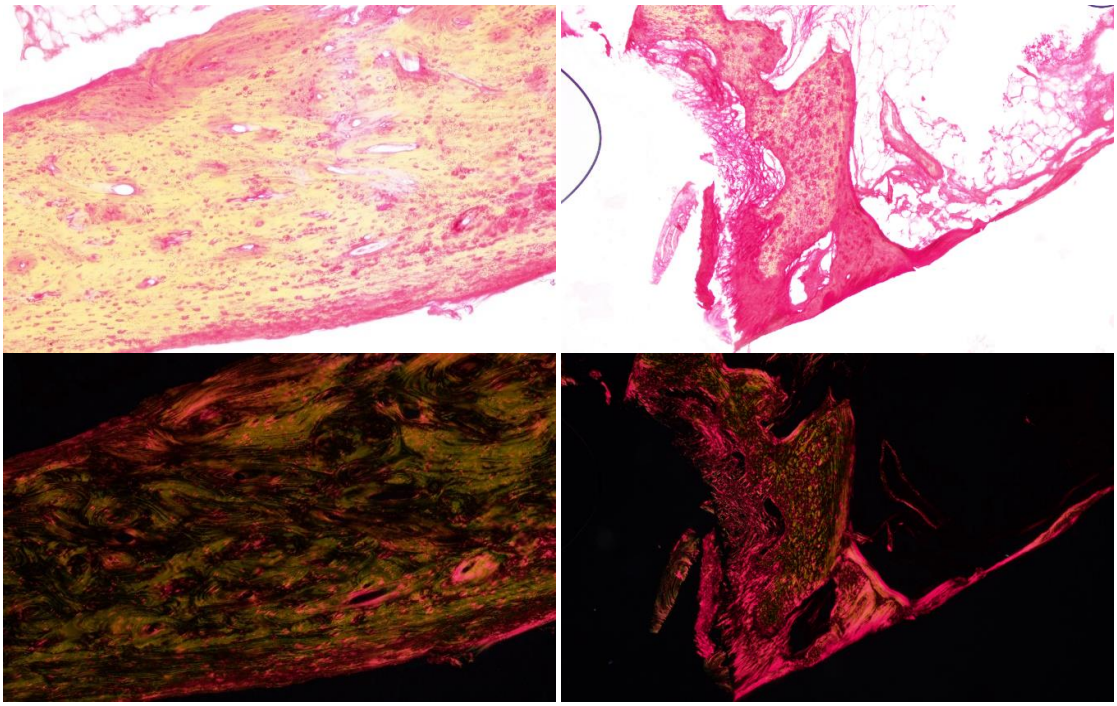

C. Red-green pixel ratio

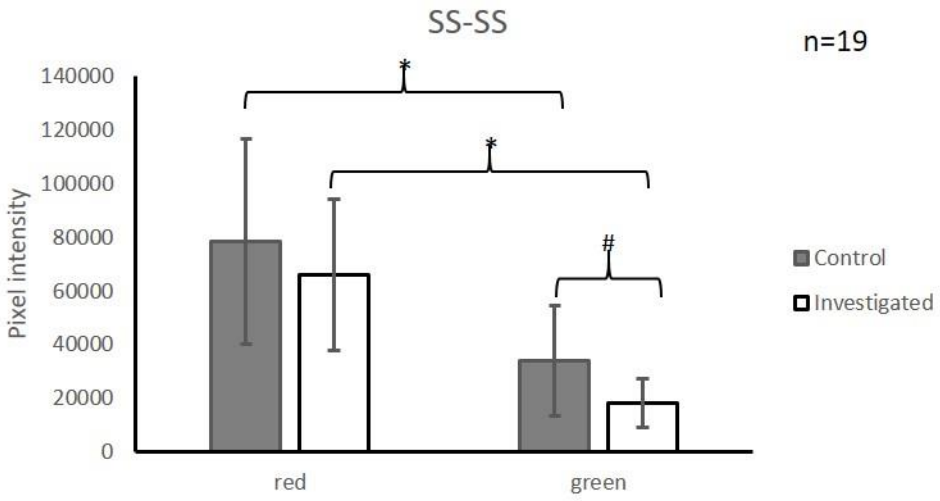

Figure 19. Examination of the organic matrix production of bone. Hematoxilin eosin (A) and picrosirius red (B) staining. Original magnification was 20×. Scale bar: 100 μm. Optical density (OD) of red and green pixels was determined in micrographs and normalised to control, unoperated bone samples (C). Asterisks indicate significant (*p<0.05) change in red or green pixel intensity compared to the corresponding control and (#p<0.05) change in red-red or green-green compared to the corresponding control in stainless steel-stainless steel group.

4.3. Titanium-stainless steel group

In the intact bone of the Ti-SS experimental group, some morphological changes were detected (Figure 20.A) and intensive callus formation was shown on the Titanium screw side (Figure 20.A). nterestingly, picrosirius staining showed a stronger red colour in polarised light on the studied side (Figure20.B). After surgery between titanium and stainless steel (Ti-SS) screws, a significant increase in the amount of thick collagen fibres was detected, but no change in the amount of thin collagen fibres was shown in the control or studied side (Figure 20.C).

A. H&E staining

Control Investigated

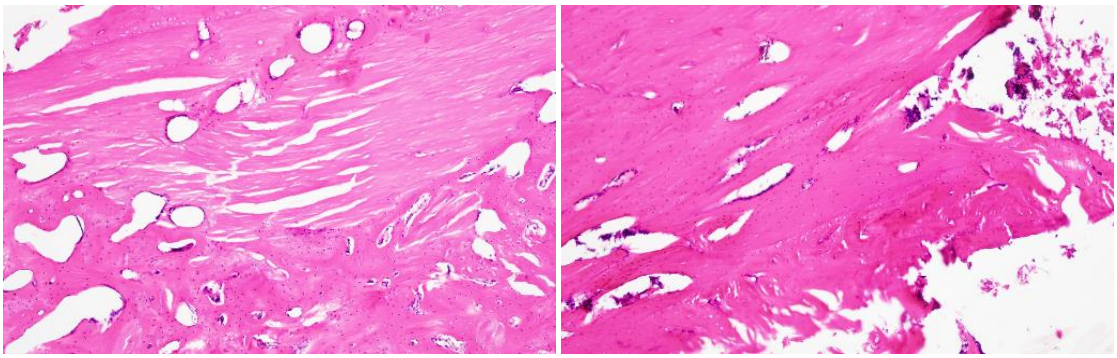

B. Picrosirius red staining

Control Investigated

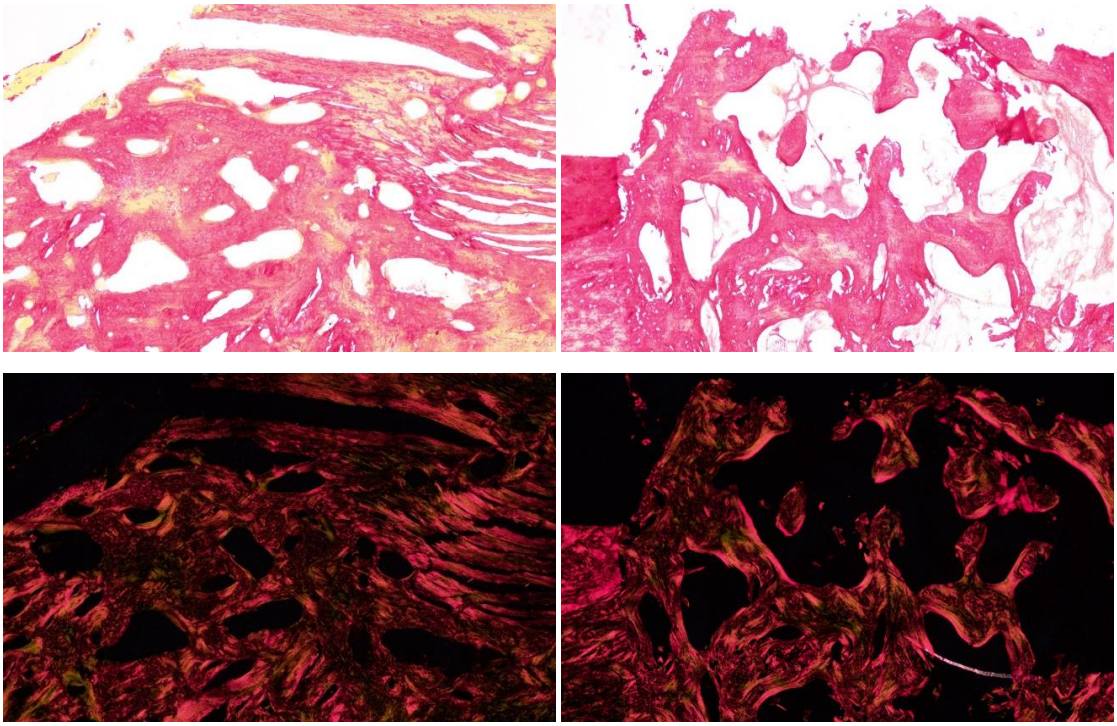

C. Red-green pixel ratio

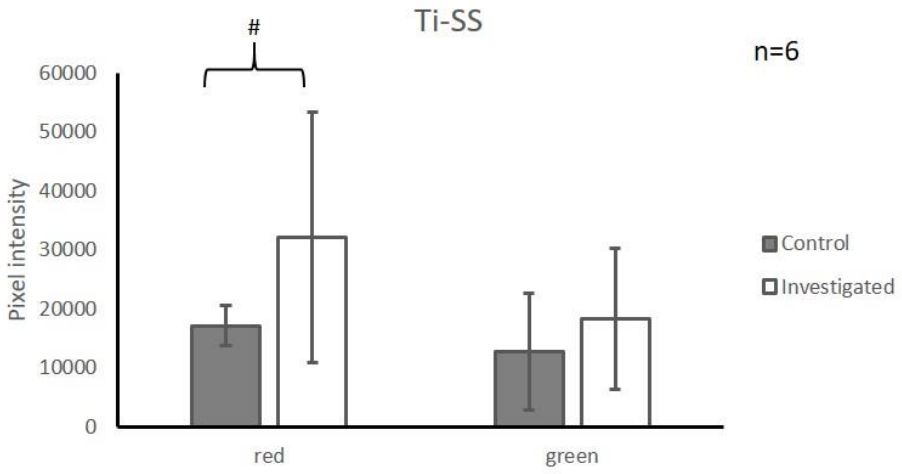

Figure 20. Examination of the organic matrix production of bone. Hematoxilin eosin (A) and picrosirius red (B) staining. Original magnification was 20×. Scale bar: 100 µm. Optical density (OD) of red and green pixels was determined in micrographs and normalised to control, unoperated bone samples (C). Asterisks indicate significant (*p<0.05) change in red or green pixel intensity compared to the corresponding control and (#p<0.05) change in red-red or green-green compared to the corresponding control in titanium-stainless steel group.

4.4. Gold-stainless steel group

The use of gold screws did not alter normal callus formation (Figure 21.A) and did not alter the amount of red and green fibres in control and callus bones (Figure 21.B). On the other hand, a decreased amount of thin fibres was detected in both control and operated cortical bone (Figure 21. C), as is seen under normal conditions. No significant changes were observed in the amount of either thick or thin collagen fibres between the intact cortical bone and the gold screw side (Figure 21.C).

A. H&E staining

Control Investigated

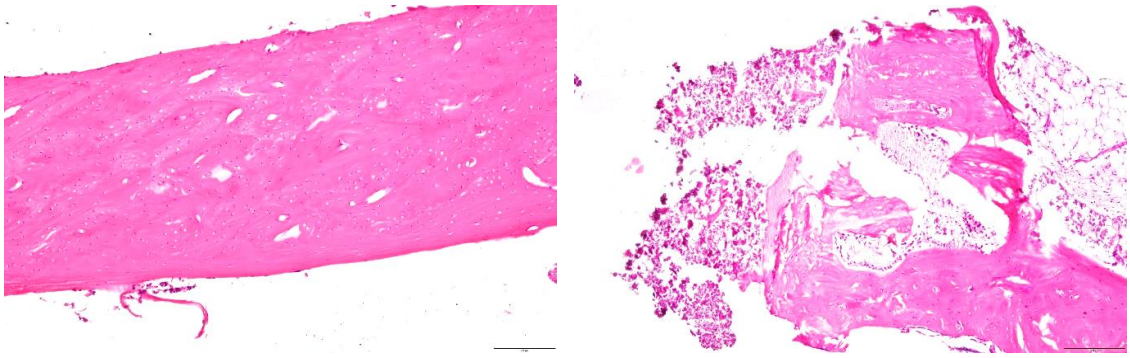

B. Picrosirius red staining

Control Investigated

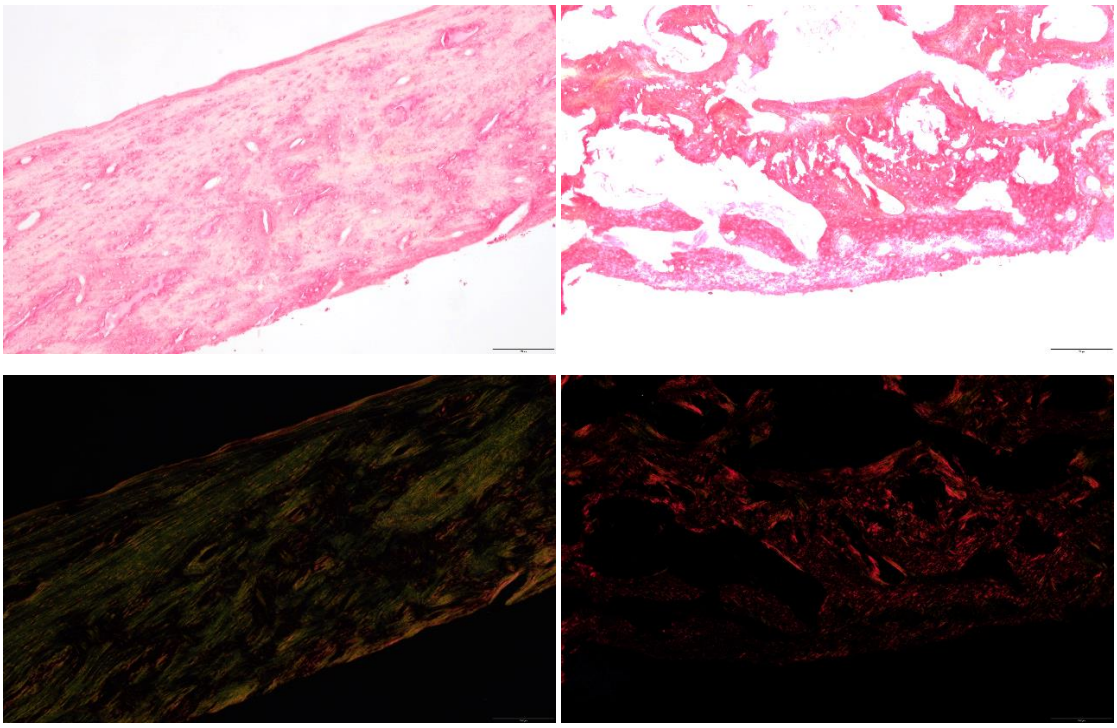

C. Red-green pixel ratio

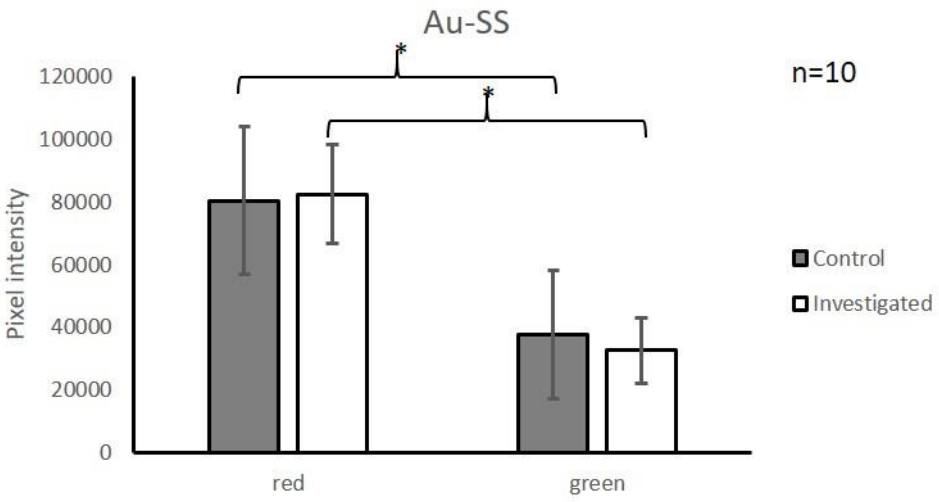

Figure 21. Examination of the organic matrix production of bone. Hematoxilin eosin (A) and picrosirius red (B) staining. Original magnification was 20×. Scale bar: 100 μm. Optical density (OD) of red and green pixels was determined in micrographs and normalised to control, unoperated bone samples (C). Asterisks indicate significant (*p<0.05) change in red or green pixel intensity compared to the corresponding control and (#p<0.05) change in red-red or green-green compared to the corresponding control in titanium-stainless steel group.

4.5. Platinum-stainless steel group

The Platinum screw application showed normal callus formation (Figure 22.A) without any morphological disturbance. In the normal light of picrosirius staining, a stronger red colour was detected in the bone on the Platinum screw side (Figure 22.B). Furthermore, a significant increase in the presence of thick and thin collagen was noted on the side of the platinum screws (Figure 22.C).

A. H&E staining

Control Investigated

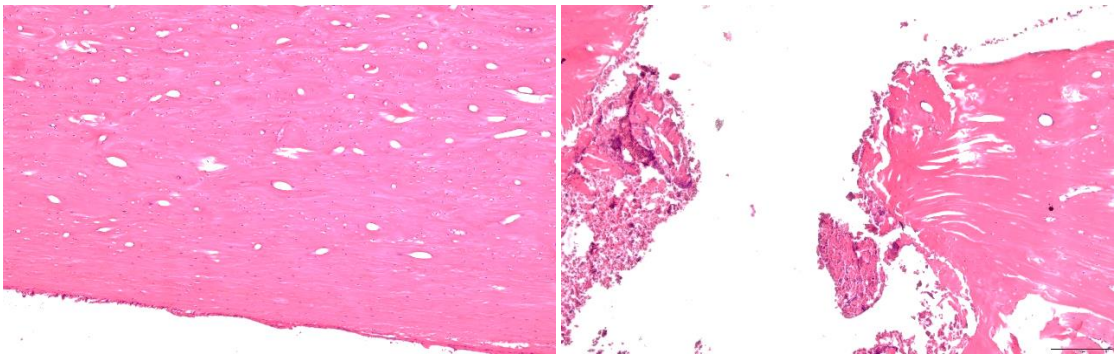

B. Picrosirius red staining

Control Investigated

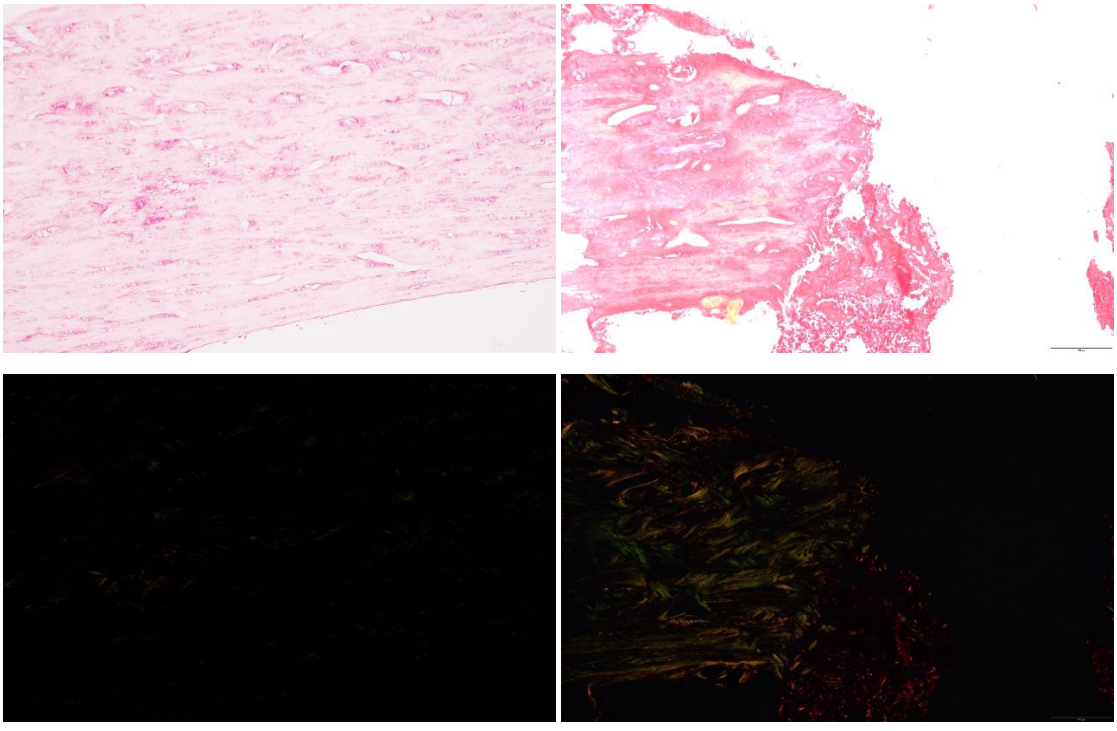

C. Red-green pixel ratio

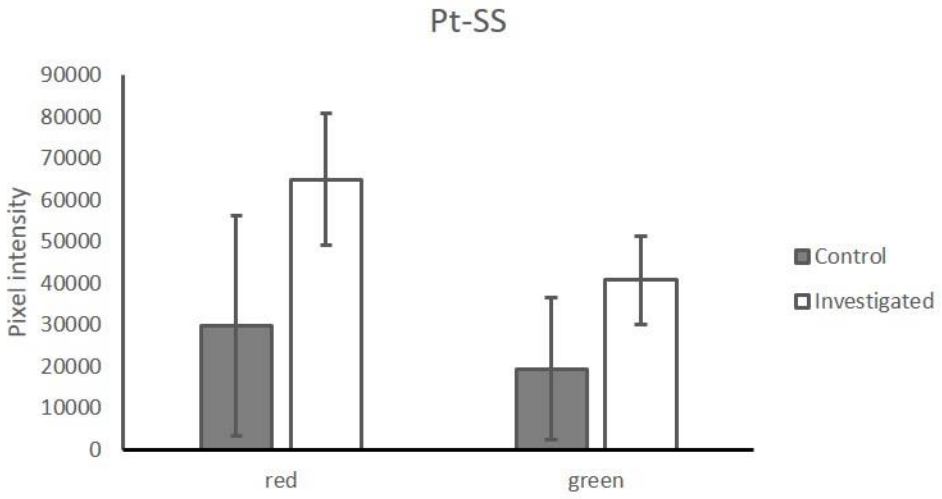

Figure 22. Examination of the organic matrix production of bone. Hematoxilin eosin (A) and picrosirius red (B) staining. Original magnification was 20×. Scale bar: 100 μm. Optical density (OD) of red and green pixels was determined in micrographs and normalised to control, unoperated bone samples (C). Asterisks indicate significant (*p<0.05) change in red or green pixel intensity compared to the corresponding control and (#p<0.05) change in red-red or green-green compared to the corresponding control in platinum-stainless steel group.

5. Genes expressions

Materials and methods

Bone powder obtained after grinding surgically removed rabbit bone samples in liquid nitrogen was first isolated for RNA isolation. The isolation yielded measurable amounts of RNA for all samples. The amount of RNA in the samples was determined using a NanoDrop One spectrophotometer (ThermoFisher Scientific). In all cases, the same amount of template RNA was used for cDNA synthesis using the High-Capacity cDNA Reverse Transcription Kit (Applied Biosystems). Real-time qPCR analysis following reverse transcription was performed to determine the expression levels of genes involved in bone formation (RUNX2, BMP-2, ALPL, SPP1, SP7, OCN, IBSP). For each gene, the measured expression levels were normalised to the Ct (number of cycles at a given threshold) determined for the housekeeping gene GAPDH, which was used as an internal control. Gene expression assays were performed using gene-specific TaqMan assays (Applied Biosystems) in 5x HOT FIREPOL Probe qPCR Mix Plus (no ROX) (Solis BioDyne) master mix reagent. The bar graphs showing the results of the measurements represent the relative expression levels obtained after normalisation to the internal control.

Results

Our results show that, as expected, the expression of ALP, RUNX2, SP7, among the osteoblast cell marker genes involved in bone formation, was increased in the bone defect only compared to the non-defective control sample, based on three independent measurements. Metallic probes placed in the bone did not decrease the expression of all three genes in some cases and genes, but rather decreased it in most cases (Ti-SS, SS-SS) (Figure 23.).

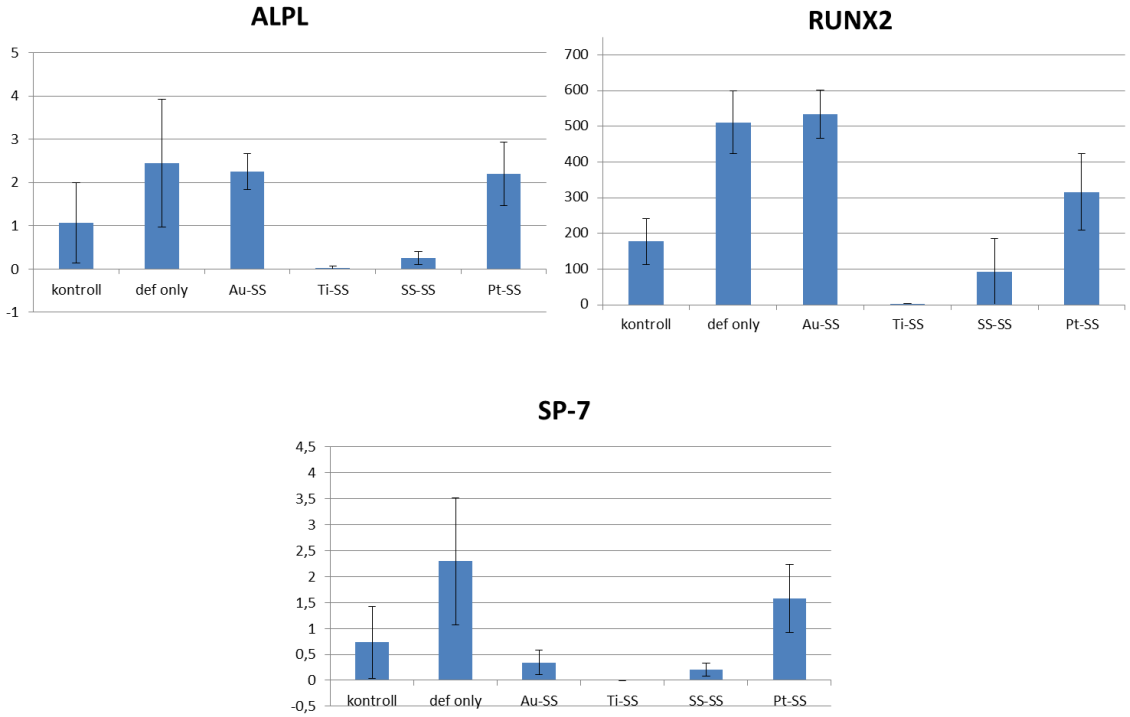

Figure 23. Expression levels of ALPL, RUNX2, SP-7 genes in control, defect only, gold-steel (Au-SS), titanium-steel (Ti-SS), steel-steel (SS-SS), platinum-steel (Pt-SS) metal-pairing treated samples.

DISCUSSION

The experiments carried out have shown that an electrical voltage is generated between metal implants placed in bone. A potential difference occurs not only between metals of different materials, but also between implants of the same material, which can be explained by the piezoelectric property of bone. The resulting potential difference makes it likely that implants will behave as galvanic elements. The potential between implants of the same material and implants of different materials varies over time. In the experiments, the voltage values shifted negatively in the first few days after bone defect creation and implantation, and then stabilised at positive values after an increase. The behaviour of the resulting stress curves was similar for all metal pairs used.

Radiographic analysis of bone healing showed the following. During the healing of the created bone defect, the size of the residual defect was almost similar for all metal pairs used. There was no difference in the volume of callus formed between the SS-SS and SS-Ti metal pairs, while the volume of callus formed was less than that for the Au-SS and Pt-SS pairs, and the bone density of the callus formed was closest to normal bone density for the Pt-SS pair. The Pt-SS metal pair therefore formed less bone, but at a density closer to physiological bone density.

Histological studies have shown that the amount of thick and thin collagen in newly formed bone is closest to the amount of physiological bone tissue used as a control during bone healing in Au-SS metal pairs. For Ti-SS and Pt-SS metal couples, an increase in thick collagen formation was observed, whereas for the Pt-SS combination no morphological difference was found, and for Ti-SS metal couples intense callus formation was observed. This confirms that the quality of the metal implanted in the bone influences the qualitative and quantitative indicators of collagen formation.

Among the genes involved in ossification, the genes ALP, RUNX2, SP7 were found to have decreased gene expression when any combination of metals was implanted compared to bone where only one defect was

created. In the case of ALPL and RUNX2, the expression of the addot genes is much closer to control for the AU-SS and Pt-SS metal combinations than for the SS-SS and SS-Ti combinations. For SP7, no significant decrease in expression is observed for the Pt-SS pairing alone.

Overall, we find that there is no negative effect on bone healing when stainless steel implants are combined with any of the metals used in the study, and some beneficial effects are seen when combined with gold and platinum implants. The potential difference is therefore unlikely to have a detrimental effect on bone healing, and in some cases a positive effect may be observed. We believe that further studies are needed to exploit this phenomenon in practical applications.

REFERENCES

1. Hayes JS, Richards RG (2010) The use of titanium and stainless steel in fracture fixation. Expert Rev. Med. Devices 7(6): 843-853.
2. Kim KT, Eo MY, Nguyen TTH, Kim SM (2019) General review of titanium toxicity. Int J Implant Dent. 5(1):10.
3. Høl PJ, Mølster A, Gjerdet NR (2008) Should the galvanic combination of titanium and stainless steel surgical implants be avoided? Injury 39:161-9.
4. Clauss M, Graf S, Gersbach S, Hintermann B, Ilchmann T, Knupp, M (2013) Material and biofilm load of K wires in toe surgery: titanium versus stainless steel. Clinical orthopaedics and related research, 471(7):2312–2317. https://doi.org/10.1007/s11999-013-2919-5
5. Moriarty T F, Debefve L, Boure L, Campoccia D, Schlegel U, Richards RG (2009) Influence of Material and Microtopography on the Development of Local Infection in vivo: Experimental Investigation in Rabbits. The International Journal of Artificial Organs 32(9):663–670. https://doi.org/10.1177/039139880903200916
6. Arens S, Schlegel U, Printzen G, Ziegler WJ, Perren SM, Hansis M (1996) Influence of materials for fixation implants on local infection. An experimental study of steel versus titanium DCP in rabbits. J Bone Joint Surg Br. 78(4): 647–651.
7. Hauke C, Schlegel U, Melcher GA (1997) Local infection in relation to different implant materials. An experimental study using stainless steel and titanium solid, unlocked intramedullary nails in rabbits. Orthop. Trans. 21:835–836.
8. Soultanis K, Pyrovolou N, et al.(2006) Instrumentation loosening and material of implants as predisposal factors for late postoperative infections in operated idiopathic scoliosis. Stud Health Technol Inf. 123:559–564.
9. Di Silvestre M, Bakaloudis G, Lolli F, Giacomini S, (2011) Late-developing infection following posterior fusion for adolescent idiopathic scoliosis. Eur Spine J.; 20(Suppl 1):S121–S127. doi:10.1007/s00586-011-1754-1
10. Rho JY, Ashman RB, Turner CH (1993) Young's modulus of trabecular and cortical bone material: ultrasonic and microtensile measurements. J Biomech. 26(2): 111–119.
11. Choi K, Kuhn JL , Ciarelli MJ, Goldstein SA (1990) The elastic moduli of human subchondral, trabecular, and cortical bone tissue and the size-dependency of cortical bone modulus. J Biomech. 23(11):1103–1113.
12. Jacobs JJ, Gilbert JL, Urban RM (1998) Corrosion of Metal Orthopaedic Implants. The Journal of Bone and Joint Surgery 80-A(2):268-282.
13. Zartman KC, Berlet GC, Hyer CF et al. (2011) Combining dissimilar metals in orthopaedic implants: revisited. Foot Ankle Spec 4(5):318-23.
14. Disegi JA, Eschbach L (2000) Stainless Steel in Bone Surgery. Injury 31(4):2-6.
15. Agins HJ, Alcock NW, Bansal M, et al. (1988) Metallic wear in failed titanium-alloy total hip replacements. A histological and quantitative analysis. J Bone Joint Surg Am 70:347—356.

16. Farnsworth CL, Newton PO, Breisch E, Rohmiller MT, Kim JR, Akbarnia BA (2014) The Biological Effects of Combining Metals in a Posterior Spinal Implant: In Vivo Model Development Report of the First Two Cases. Advances in Orthopedic Surgery 2014:1-9.
17. Black J (1988) Does corrosion matter? Journal of Bone and Joint Surgery B 70(4): 517–520.
18. Gaine WJ, Andrew M, Chadwick P, Cooke E, Williamson JB (2001) Late operative site pain with isola posterior instrumentation requiring implant removal: infection or metal reaction? Spine 26(5):583–587.
19. Serhan H, Slivka M, Albert T et al. (2004) Is galvanic corrosion between titanium alloy and stainless steel spinal implants a clincal concern? The Spine Journal. 4:379-387.
20. Acevedo D, Loy BN, Lee B et al. (2013) Mixing Implants of Differing Metallic Composition in the Treatment of Upper-extremity Fractures. Orthopedics 36(9):e1175-e1179.
21. Hallab N, Merritt K, Jacobs JJ. (2001) Metal Sensitivity in Patients with Orthopaedic Implants. The Journal of Bone and Joint Surgery 83(3):428-36.
22. Devine DM, Leitner M, Perren SM et al. (2009) Tissue Reaction to Implants of Different Metals: A Study Using Guide Wires in Cannulated Srews. European Cells and Materials 18:40-48.
23. Kim TI, Han JH, et al. (1997) New titanium alloys for biomaterials: a study of mechanical and corrosion properties and cytotoxicity. Biomed Mater Eng. 7(4):253–263.
24. Dubousset J, Shuffleberger H, Wenger D, (1994) Late infection with CD instrumentation. Orthopaedic Transactions 18:121.
25. Richards S (1995) Delayed infections following posterior spinal instrumentation for the treatment of idiopathic scoliosis. Journal of Bone and Joint Surgery A 77(4):524–529.
26. Clark CE, Shufflebarger HL, (1999) Late developing infection in instrumented idiopathic scoliosis. Spine 24(18):1909–1912.
27. Lucas LC, Dale P, Buchanan R, Gill Y, Griffin D, Lemons JE (1991) In vitro vs in vivo corrosion analyses of two alloys Journal of Investigative Surgery 4(1):13–21.
28. Cunningham BW, Orbegoso CM, Dmitriev AE et al. (2003) The effect of spinal instrumentation particulate wear debris: an in vivo rabbit model and applied clinical study of retrieved instrumentation cases. Spine Journal 3(1):19–32.
29. Hallab NJ, Cunningham BW, Jacobs JJ (2003) Spinal implant debris-induced osteolysis. Spine 28(20):S125–138.
30. Zabrzynski J, Jaworski Ł (2017). Myths and facts about combining metals in orthopedic surgery. Chirurgia narzadow ruchu i ortopedia polska. 82(1).
31. El-Zayat BF, Ruchholtz S, Efe T, Paletta J, Kreslo D, Zettl R (2013). Results of titanium locking plate and stainless steel cerclage wire combination in femoral fractures. Indian journal of orthopaedics, 47(5):454-458.
32. Beavers RN, Lall RR, Barnett JO, Desai SK (2017) Pseudarthrosis due to galvanic corrosion presenting as subarachnoid hemorrhage. Journal of craniovertebral junction & spine 8(2):156-158.
33. Fukada E, Yasuda I. (1957) On the piezoelectric effect of bone. J Phys Soc Japan 12(10):1158–62.
34. Pawlikowski, Maciej (2017) Electric Phenomenon in Bones as a Result of Piezoelectricity of Hydroxyapatite. Archives of Clinical and Biomedical Research. 1:132-139.
35. Otter M, Goheen S, Williams WS (1988) Streaming potentials in chemically modified bone. J Orthop Res. 6:346–59.
36. Rubinacci A, Black J, Brighton CT, Friedenberg ZB (1988) Changes in bioelectric potentials on bone associated with direct current stimulation of osteogenesis J Orthop Res. 6(3):335-45.
37. Martin, RB (1979). Comparison of capacitive and inductive bone stimulation devices. Ann Biomed Eng. 7(5-6):387-409.
38. Brighton CT, Friedenberg ZB, Mitchell EI, Booth RE (1977). Treatment of Nonunion with Constant Direct Current. Clinical orthopaedics and related research. 124:106-123.
39. Sharrard W (1990). A Double-blind trial of pulsed Electromagnetic Fields for delayed union of tibial fractures. J Bone Joint Surg Br. 72(3):347-55.
40. Brighton CT, Black J, Friedenberg Z, Esterhai JL, Day LJ, Connolly JF. (1981) A multicenter study of the treatment of non-union with constant direct current. J Bone Joint Surg. 63:2–13.

41. Mollon B, da Silva V, Busse JW, Einhorn TA, Bhandari M. (2008) Electrical stimulation for long-bone fracture-healing: a meta-analysis of randomized controlled trials. J Bone Joint Surg Am. 90:2322–30.
42. Paterson DC, Lewis GN, Cass CA (1980) Treatment of delayed union and nonunion with an implanted direct current stimulator. Clin Orthop Relat Res. 148:117-28.
43. Brighton CT. (1981) Treatment of nonunion of the tibia with constant direct current (1980 Fitts Lecture, A.A.S.T.). J Trauma 21(3):189-95.
44. Brighton CT, Friedenberg ZB, Mitchell EI, Booth RE. (1977) Treatment of nonunionwith constant direct current. Clin Orthop Relat Res. 124:106-23.
45. Esterhai JL Jr, Brighton CT, Heppenstall RB,Thrower A (1986) Nonunion of the humerus. Clinical, roentgenographic, scintigraphic, and response characteristics to treatment with constant direct current stimulation of osteogenesis. Clin Orthop Relat Res. 211:228-34.
46. Hughes MS, Anglen JO (2010) The use of implantable bone stimulators in nonunion treatment. Orthopedics 33(3):151-7.
47. Gan JC, Glazer PA (2006) Electrical stimulation therapies for spinal fusions: current concepts. Eur Spine J. 15:1301–11.
48. Saxena A, DiDomenico LA, Widtfeldt A, Adams T, Kim W (2005) Implantable electrical bone stimulation for arthrodeses of the foot and ankle in high-risk patients: a multicenter study. J Foot Ankle Surg. 44:450–454.